PCCP

PAPER

Cite this: *Phys. Chem. Chem. Phys.*, 2020, **22**, 26372

Solvent effects on triplet–triplet annihilation upconversion kinetics of perylene with a Bodipy-phenyl-C_{60} photosensitizer†

Yaxiong Wei, [ab] Ye Wang,[cd] Qiaohui Zhou,[a] Song Zhang, *[cd] Bing Zhang,[cd] Xiaoguo Zhou *[a] and Shilin Liu [a]

Received 10th August 2020,
Accepted 25th October 2020

DOI: 10.1039/d0cp04230g

rsc.li/pccp

The solvent effect usually plays an important role in triplet–triplet annihilation (TTA) upconversion processes. In this work, we have studied the TTA upconversion kinetics of perylene with Bodipy-phenyl-C_{60} as the triplet photosensitizer in five solvents, 1,4-dioxane, dichlorobenzene, chlorobenzene, toluene, and tetrahydrofuran (THF). Although no significant solvent effect was observed in steady-state absorption and fluorescence emission spectra, the overall TTA upconversion quantum yields showed a profound dependence on solvent properties, *i.e.* 4.9% in 1,4-dioxane, 7.1% in dichlorobenzene, 6.7% in chlorobenzene, 4.6% in toluene, and 2.2% in THF (the maximum of 50%). Each elementary reaction step involved in the overall process was analyzed by applying femtosecond and nanosecond time-resolved transient absorption spectroscopy, revealing that the fluorescence emission of perylene was more significantly affected by the solvents in contrast to the other steps. Moreover, an extra intramolecular energy-transfer pathway of Bodipy-phenyl-C_{60} was found *via* the formation of charge-separated states in dichlorobenzene, chlorobenzene, and THF solvents, once being excited. These conclusions provide valuable clues to choose the most favorable solvent for the higher TTA upconversion efficiency in related applications.

1 Introduction

Photon upconversion based on triplet–triplet annihilation (TTA) of organic molecules as triplet photosensitizers is highly attractive for photovoltaic, photocatalysis, and other related fields, in which the absorbed photons with lower energy can be converted to higher energy photons for emission in a suitable system that consisted of triplet photosensitizers and acceptors.[1–3]

During the past decades, many efforts have been made to develop efficient photosensitizers for TTA upconversion. Metal–organic complexes are the most widely used photosensitizers,[4–6] such as polyimine Ru(II), cyclometalated Ir(III), Pt(II)/Pd(II) porphyrin, and Os(II) phenanthroline complexes. Thanks to the heavy atom effect induced by transition metals,[7,8] the long-lifetime triplet photosensitizers can be formed *via* intersystem crossing (ISC) after photoexcitation, promoting the observable TTA upconversion emission.[9] However, the expensive transition-metal complexes usually have relatively weak absorption in the visible light range, compared with traditional chromophores such as rhodamine, Bodipy, *etc.*[10] Metal-free triplet photosensitizers have been used in TTA upconversion and sensitize singlet oxygen,[11] such as bromo- or iodo-Bodipy, thermally activated delayed fluorescence molecules, and organic π-radical molecules. Recently, several dyad photosensitizers with fullerene ligands have been synthesized and applied for TTA upconversion, in which the C_{60} and C_{70} ligands play the role of spin converters due to their approximately 100% ISC efficiencies.[12–14] As shown in the scheme of Fig. 1a, the representative TTA upconversion using the dyad photosensitizers contains five elementary reaction steps after photo-absorption: intramolecular singlet energy transfer (ET) from a light harvester moiety to a fullerene ligand, ISC of the fullerene moiety, triplet–triplet energy transfer (TTET) to produce triplet acceptors, TTA of two triplet acceptors to form one singlet-excited acceptor, and fluorescence (FL) emission of a singlet acceptor.

[a] *Hefei National Laboratory for Physical Sciences at the Microscale, Department of Chemical Physics, University of Science and Technology of China, Hefei, Anhui 230026, China. E-mail: xzhou@ustc.edu.cn*
[b] *College of Materials Science and Engineering, Shenzhen University, Shenzhen, Guangdong, 518060, China*
[c] *State Key Laboratory of Magnetic Resonance and Atomic and Molecular Physics, Innovation Academy for Precision Measurement Science and Technology, Chinese Academy of Sciences, Wuhan 430071, China*
[d] *University of Chinese Academy of Sciences, Beijing 100049, China. E-mail: zhangsong@wipm.ac.cn*

† Electronic supplementary information (ESI) available: Femtosecond and nanosecond time-resolved transient absorption spectra, steady-state absorption and fluorescence emission of perylene itself in different solvents, the decay curve of C_{60}-Bodipy in different concentrations of perylene with different solvents and DFT calculation data. See DOI: 10.1039/d0cp04230g

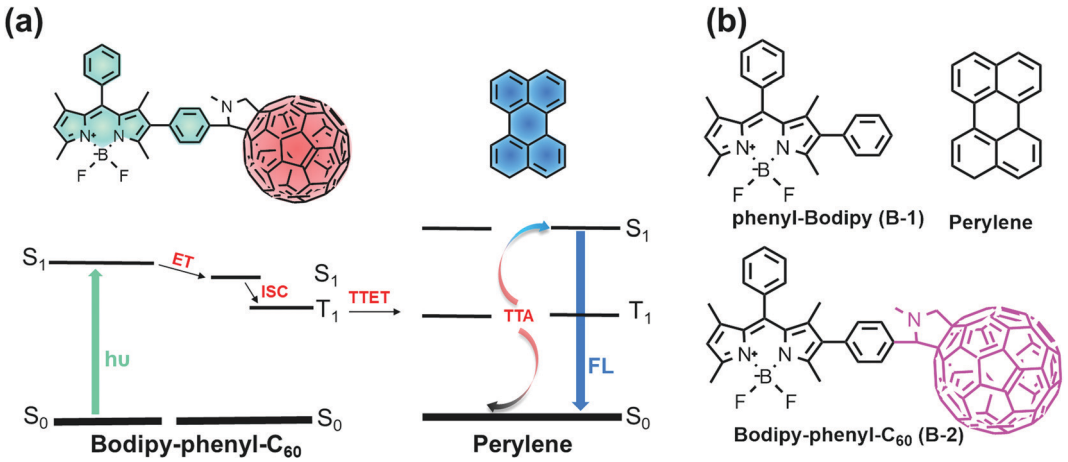

Fig. 1 (a) Scheme of TTA upconversion kinetics in Bodipy-phenyl-C_{60} and perylene and (b) structures of perylene and light antennas, phenyl-Bodipy (**B-1**) and Bodipy-phenyl-C_{60} (**B-2**).

Considering the rigorous energy rule for triplet acceptors, like perylene, where the double energy of the triplet state needs to be slightly higher than its singlet energy,[15,16] solvent effects must play an important role in the overall TTA upconversion kinetics. In general, the viscosity of solvent may alter bio-molecular reaction rates due to different collision ability, *e.g.* TTET and TTA. Murakami *et al.*[17,18] observed the dependence of the TTA upconversion yield on the viscosity of ionic solution. The improved triplet fusion yield with the increase of solvent viscosity was also reported by Yokoyama *et al.*[19] Castellano *et al.* obtained an unprecedented upconversion quantum yield of 15.5% (the maximum of 50%) with BPEA as an acceptor in high viscous PEG solution,[20] while this yield was only 1.6% in low viscosity solvent (toluene).[21] These results indicated that the encounter complexes formed upon collision between annihilators had a longer lifetime in high viscosity solvent, which could improve the TTA efficiency.[21] Moreover, solvent effects on the TTA upconversion of perylene were also reported by Ye *et al.*,[22] that the TTA efficiency was increased in higher-viscosity solvents, meanwhile the low-polarity solvents were better for TTA upconversion due to the lower amount of excimer emission. In contrast, solvent polarity can remarkably affect ISC rates and fluorescence quantum yields by changing the energy gap between ground and excited states,[23] but it has been rarely mentioned in previous TTA upconversion studies. Recently, we have studied the TTA upconversion of perylene in hexane, heptane, toluene, dioxane and DMSO with the I_2-Bodipy photosensitizer.[24] The quenching rate constant of triplet $^3I_2$-Bodipy* was completely controlled by solvent viscosity, whilst, a more significant solvent effect was found in the TTA process and fluorescence emission of perylene. It is worth noting that the influences of solvent viscosity and polarity on TTA upconversion kinetics are not independent, and it is necessary to be carefully checked in each system to optimize conditions for the highest upconversion efficiency.

In the TTA upconversion system of perylene using Bodipy-phenyl-C_{60} (**B-2** in Fig. 1b) as the triplet photosensitizer, the quantum yields of ET, ISC, and TTET processes were measured respectively in toluene, and the overall quantum yield of the TTA upconversion, Φ_{UC}, was determined to be 2.9% (the maximum of 50%).[12] Although the yield was just passable, it was far below our expectations. The inappropriate solvent might be a dominant reason. Therefore, we have reinvestigated the TTA upconversion kinetics in five solvents: 1,4-dioxane, toluene, chlorobenzene, *o*-dichlorobenzene and THF. The quantum yield of each elementary reaction step was measured using transient absorption spectroscopy and fluorescence emission spectroscopy. Cyclic voltammetry was also conducted to assess a potential electron-transfer mechanism. The complex solvent effects were unveiled in the overall TTA upconversion kinetics of perylene using a **B-2** photosensitizer.

2 Experimental and computational

2.1 Synthesis and characterization

As shown in Fig. 1b, a C_{60} group was linked to the core of the fluorophore by a phenyl bridge in **B-2**. The details of the synthetic process were described in previous work.[12]

2.2 Experimental setups

The steady-state UV-Vis absorption spectra were recorded in the wavelength range of 300–800 nm with a spectrophotometer (UV-3600, Shimadzu). The fluorescence emission spectra were measured with a fluorescence spectrophotometer (F-4600, Hitachi) in the wavelength range of 400–800 nm.

Femtosecond time-resolved transient absorption spectra were measured with a pump–probe strategy as described previously.[12] An excitation femtosecond laser with 35 fs pulse width was generated at 532 nm from NOPA, with an attenuated energy of about 4.5 μJ. Meanwhile, a fraction of the pump laser was focused on a CaF_2 plate to produce a white light continuum as the probe laser. The relative polarization of the pump and probe pulses was maintained as 54.7°. The absorption spectra were recorded with a CCD camera equipped with a spectrometer (Princeton, SpectraPro 2500i). The instrumental response function was better than 150 fs.

A home-built laser flash photolysis system was used to measure nanosecond transient absorption spectra. The second harmonic 532 nm of a Q-Switched Nd:YAG laser (PRO-190, Spectra Physics) was used as the excitation light (pulse duration 8 ns, repetition rate of 10 Hz, and pulse energy <10 mJ per pulse). The analyzing light was a 500 W xenon lamp, and intersected with the pulsed laser in a quartz cuvette (10×10 mm) at right angles. A monochromator (Omni-λ 5025) equipped with a photomultiplier (CR131, Hamamatsu) was used to record the transient absorption spectra within the wavelength range of 300–800 nm, with a spectral resolution of better than 1 nm. A decay curve of the intermediate was averaged by multi-shots and recorded with an oscilloscope (TDS3052B, Tektronix). All solutions were deoxygenated by purging with high purity argon (99.99%) for more than 20 minutes prior to measurements.

In experiments of TTA upconversion spectra, the mixed solution of the photosensitizer and acceptor in a quartz cuvette (10×10 mm) was deoxygenated for at least 20 minutes. A CW 532 nm laser was used as the excitation light source, where the light spot diameter was *ca.* 5 mm. The fluorescence was dispersed using a triple monochromator system (TriplePro, Acton Research), and was recorded using a CR131 photomultiplier. The spectral resolution was ~1.0 nm. As recently discussed by Zhou *et al.*,[25] the maximum upconversion quantum yield was set to be 50% in the following discussions.

Density functional theory (DFT) was applied to optimize the geometries of the photosensitizer and acceptor in ground and excited states, with the B3LYP functional and 6-31G(d) basis set. No imaginary frequencies were confirmed for all optimized structures. The spin density surface of the dyad was analyzed to verify the properties of triplet states. Moreover, the excited energies of singlet and triplet states were calculated at the same level. The vertical excitation energies were directly compared with the experimental absorption spectra. The PCM model was used to evaluate solvent effects on energy gaps between the ground state and the triplet excited states. All these calculations were performed with the Gaussian 09W program package.[26]

3 Results and discussion

3.1 Steady-state absorption and fluorescence spectra

Fig. 2 shows steady-state UV-Vis absorption spectra of **B-1** and **B-2** in five solvents. Both **B-1** and **B-2** had strong absorptions in the region of 450–550 nm. In these solvents, absorption intensities of the two molecules did not significantly change, as the maximal molar extinction coefficients (ε) were *ca.* 8.7×10^4 M^{-1} cm^{-1}. The resonance absorption wavelengths showed a minor shift, due to the delocalization of the π-conjugated electrons affected by solvent polarity. With the increase of polarity, the resonance wavelength was slightly blue-shifted, indicating that the ground states of **B-1** and **B-2** were more dipolar than the corresponding excited state ($\mu_g > \mu_e$). The conclusions agree with previous results.[27]

The fluorescence emission spectra of **B-1** and **B-2** under excitation at 532 nm were also recorded and are shown in Fig. 2. **B-1** in all solvents showed strong emission in the region of 500–650 nm, and the fluorescence yields, Φ_F, were in the range of 0.81–0.94. When C_{60} was connected to the light-harvesting antenna of **B-1**, the fluorescence emission of **B-2** was almost entirely quenched. The Φ_F values were less than 0.01 (only 0.0036–0.0061 in Table 1). As proposed in previous studies,[12] an intramolecular energy transfer could quickly lead to the formation of a Bodipy-phenyl-$^1C_{60}$* dyad after photo-absorption of the Bodipy unit, and subsequently, the triplet Bodipy-phenyl-$^3C_{60}$* was formed owing to the high ISC efficiency (close to unity) of C_{60}.[28,29] Since the Bodipy moiety and the C_{60} unit in **B-2** are connected by one phenyl, each of them maintains relatively independent properties, as indicated in the absorption spectra of Fig. 2. Therefore, the intramolecular energy transfer efficiency can be calculated using eqn (1),[30]

$$\Phi_{ET} = 1 - \frac{\Phi_{da}}{\Phi_d} = \frac{k_{ET}}{k_{FL} + k_{IC} + k_{ET}} \quad (1)$$

where Φ_{da} and Φ_d are the fluorescence quantum yields of **B-2** and **B-1**, respectively. Thus, the Φ_{ET} values of the dyad were calculated

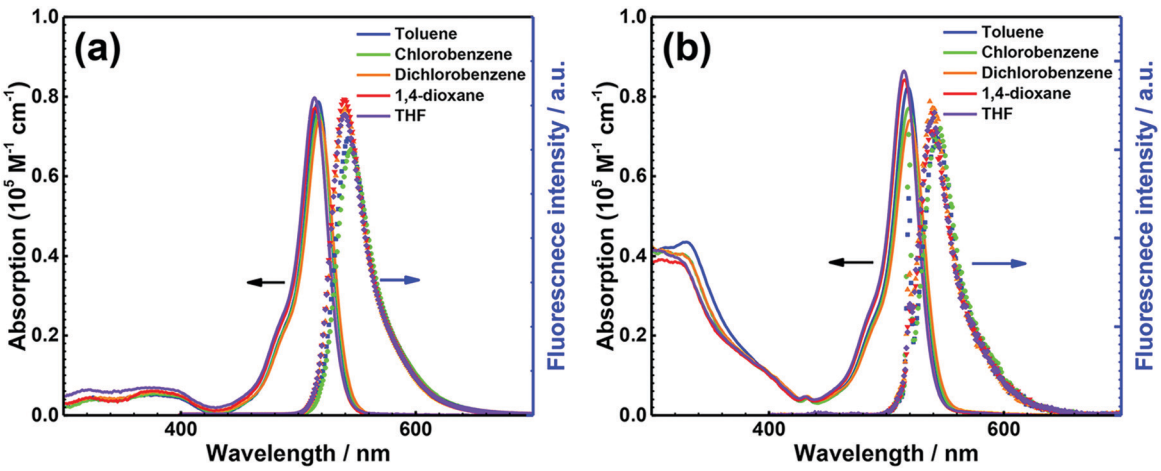

Fig. 2 Steady-state UV-Vis absorption (solid lines) and fluorescence emission (dotted lines with λ_{ex} = 532 nm) spectra in five solvents, 1,4-dioxane, toluene, chlorobenzene, dichlorobenzene, and THF. (a) **B-1** and (b) **B-2**. $c = 1 \times 10^{-5}$ M, 25 °C.

Table 1 Photophysical parameters of **B-1** and **B-2** in different solvents

Compound	Solvent	Polarity	λ_{abs}/nm	ε^a	λ_{em}/nm	$\Phi_F{}^b$/%
B-1	Toluene	2.4	517	7.9	542	82
	Chlorobenzene	2.7	517	7.6	543	82
	Dichlorobenzene	2.7	518	7.4	545	81
	THF	4.2	514	8.0	540	94
	1,4-Dioxane	4.8	514	7.7	539	92
B-2	Toluene	2.4	518	8.2	542/712	0.36
	Chlorobenzene	2.7	519	7.7	543/714	0.55
	Dichlorobenzene	2.7	520	7.4	544/715	0.61
	THF	4.2	515	8.7	538/713	0.37
	1,4-Dioxane	4.8	515	8.4	539/711	0.47

[a] Molar extinction coefficient ε was measured at maximal absorption wavelength, and the unit was 10^4 M^{-1} cm^{-1}. [b] Fluorescence quantum yield, Φ_F, was calculated using I_2-Bodipy as the standard, Φ_F (I_2-Bodipy) = 2.7% in acetonitrile.

to be all close to unity, *e.g.* 0.996 in toluene, 0.993 in chlorobenzene, 0.993 in dichlorobenzene, 0.995 in 1,4-dioxane, and 0.996 in THF (Table 1). Apparently, no visible solvent effect was found in the intramolecular energy transfer process.

3.2 Intramolecular energy transfer mechanism of B-2

Besides the direct singlet energy transfer, charge transfer also probably occurs for the ^{1}Bodipy*-phenyl-C_{60} dyad to cause energy transfer *via* a subsequent charge recombination.[31,32] Thus, cyclic voltammetry (CV) of the photosensitizer was conducted in deaerated DCM solution to analyze this probability. Fig. 3 shows the recorded CV curves of C_{60} monomers, **B-1** and **B-2**, with a scan rate of 50 mV s^{-1}. A three-electrode electrolytic cell was used, with 0.1 M tetrabutylammonium hexafluorophosphate ($Bu_4N[PF_6]$) as supporting electrolyte. The working electrode was a glassy carbon electrode, and the counter electrode was a platinum electrode. A nonaqueous $Ag/AgNO_3$ (0.1 M in acetonitrile) reference electrode was contained in a separate compartment connected to the solution *via* a semipermeable membrane. Ferrocene was added as the internal reference. As shown in Fig. 3, **B-2** has a reversible oxidation wave at 1.14 V and four reversible reduction waves at −0.79, −1.18, −1.32 and −1.71 V. Compared with the CV curves of **B-1** and C_{60} (Table S1, ESI†), the oxidation wave at 1.14 V and the reduction wave at −1.32 V can be easily attributed to the Bodipy unit, while the other three oxidation waves are contributed by the C_{60} unit.[32] Thus, the Bodipy and C_{60} units in the dyad can play the roles of an electron donor and acceptor, respectively.

To evaluate the possibility of photoinduced charge/electron transfer in the dyad, Gibbs free-energy change, ΔG_{CS}, was calculated with the Weller equations (details are introduced in the ESI†). In the nonpolar solvents, the ΔG_{CS} values were +0.18 eV in 1,4-dioxane, and +0.17 eV in toluene, indicative of a forbidden electron transfer. However, the electron transfer became allowed in the polar solvents, according to the negative ΔG_{CS} values, *e.g.* −0.39 eV in chlorobenzene, −0.45 eV in dichlorobenzene, and −0.49 eV in THF. Moreover, the energy of the charge-separated state, E_{CCS}, was calculated at the B3LYP/6-31G(d) level of theory, *e.g.* 2.52 eV in 1,4-dioxane, 2.51 eV in toluene, 1.95 eV in chlorobenzene, 1.93 eV in dichlorobenzene, and 1.89 eV in THF (Table S2, ESI†). In comparison to the S_1 state energy of the dyad (~2.39 eV), the fall in E_{CCS} with the increase of solvent polarity apparently explains whether the charge transfer occurs in thermochemistry. The simplified Jablonski diagram in Fig. 4 describes these involved elementary processes.

Although the electron transfer of the dyad was allowed in polar solvents, no experimental evidence was found in the absorption and fluorescence spectra. To clarify this inconsistency, femtosecond time-resolved transient absorption spectroscopy was performed for **B-2** in the five solvents. Since all spectra in five solvents are very similar (Fig. S1–S5, ESI†), Fig. 5a only shows the representative spectra in toluene. Besides a strong ground-state bleaching (GSB) peak in the region of 460–600 nm, a positive band was observed at 423 nm and attributed to the excited state absorption (ESA) of **B-2**, $S_n \leftarrow S_1$, while the wide band at roughly 700 nm was gradually formed with time and was predominantly assigned to the characteristic absorption of the $^3C_{60}$* unit.[12] It was reported that the absorption of the Bodipy$^+$ unit was located in the present GSB range,[33,34] and the characteristic absorption of the

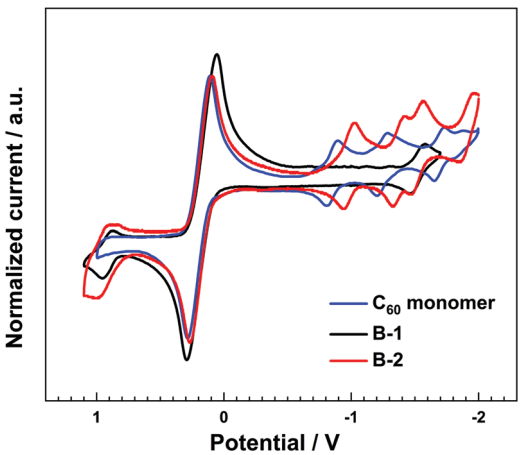

Fig. 3 Cyclic voltammograms of C_{60}, **B-1** and **B-2** in deaerated DCM solution.

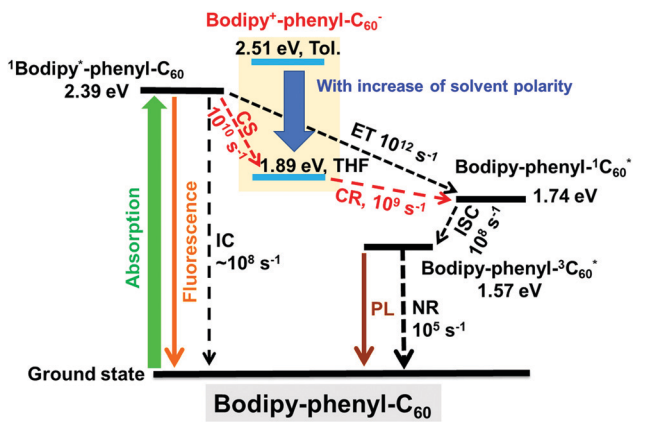

Fig. 4 Simplified Jablonski diagram for photophysical processes of **B-2** (in toluene and THF), where CS represents the charge separated process, and CR indicates the charge recombination.

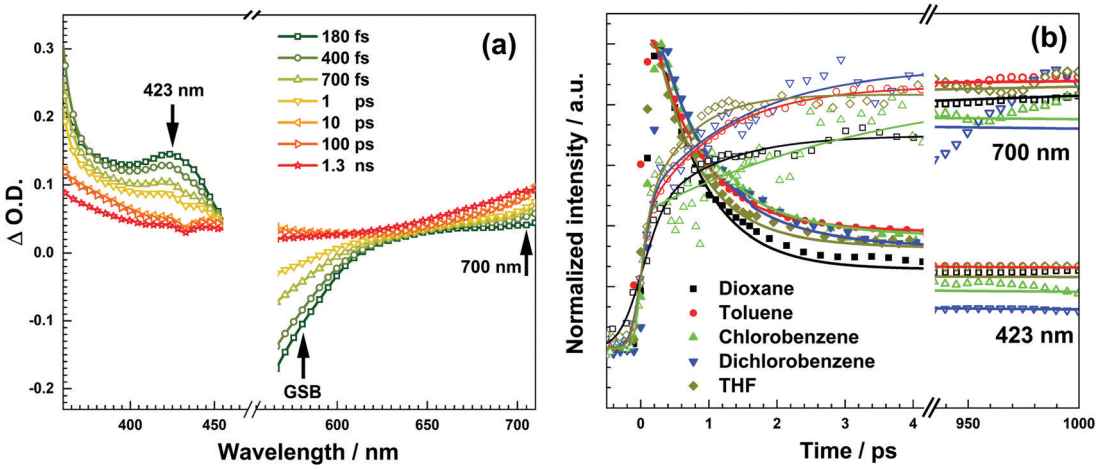

Fig. 5 (a) Femtosecond time-resolved transient difference absorption spectra of **B-2** in toluene. (b) The experimental (dotted lines) and fitted (solid lines) dynamic curves of the absorption bands at 423 and 700 nm in five solvents, 1,4-dioxane, toluene, chlorobenzene, dichlorobenzene, and THF, with photoexcitation at 532 nm (25 °C).

C_{60}^- unit was at 1020 nm.[34,35] Thus, the absorptions of both charged units were out of the present wavelength range. However, we still could provide definite evidence of charge-separated states by comparing decay kinetics of the dyad in the S_1 state in the five solvents.

Fig. 5b plots the experimental and fitted dynamic curves at 423 and 700 nm of **B-2** in the five solvents. According to the decay mechanism in Fig. 4, the attenuation process of **B-2** in the S_1 state involves four major competing processes, *i.e.* fluorescence emission, internal conversion of the Bodipy unit, charge-separated decay, and singlet energy transfer from the Bodipy core to the C_{60} moiety. Therefore, the dominant attenuation rates at 423 nm can be obtained by a multi-exponential fitting and listed in Table 2. As previously reported,[12] the fastest one with a rate ($1/\tau_1$) of *ca.* 10^{12} s^{-1} proceeds along the singlet energy transfer to form Bodipy-phenyl-$^1C_{60}$*, while the slowest internal conversion rate ($1/\tau_3$) of the dyad was around 10^8 s^{-1}. Moreover, a multi-exponential rise rate of the absorption at 700 nm was also derived from the kinetic fitting. An ultrafast formation process with a rate of 10^{12} s^{-1} definitely indicated the formation of Bodipy-phenyl-$^1C_{60}$*, and a much slower one with a 10^8 s^{-1} rate was identified to verify the following ISC rate of the C_{60} unit (Table S6, ESI†). As indicated by $1/\tau_1$ in Table 2, the intramolecular singlet energy transfer of **B-2** is relatively insensitive to solvents. This conclusion is reasonable according to the Förster singlet energy transfer theory, since the fluorescence quantum yield and lifetime of the donor (Bodipy unit), and the fluorescence spectra of the donor (C_{60} unit) did not significantly change. Furthermore, the ISC efficiency of C_{60} in solvents was reported to be close to 100%,[29,36,37] and the ISC rate of the C_{60} monomer was up to 3×10^{10} s^{-1}.[38] In contrast to the C_{60} monomer, a much slower ISC rate of the C_{60} unit in **B-2** indicated a reduced spin–orbit coupling in the dyad.

Table 2 Decay rates of the transient absorption band of **B-2** at 423 nm in different solvents

Solvent	ε (25 °C)[a]	$1/\tau_1$ (s^{-1})	$1/\tau_2$ (s^{-1})	$1/\tau_3$ (s^{-1})
1,4-Dioxane	2.21	1.44×10^{12}	—	1.05×10^8
Toluene	2.24	1.43×10^{12}	—	1.42×10^8
Chlorobenzene	5.65	1.35×10^{12}	5.62×10^{10}	2.22×10^8
Dichlorobenzene	6.83	1.28×10^{12}	6.10×10^{10}	4.05×10^8
THF	7.58	1.49×10^{12}	8.85×10^{10}	0.63×10^8

[a] Dielectric constants of solvents.

It was very interesting that there was another attenuation pathway for the excited **B-2** in polar solvents like chlorobenzene, dichlorobenzene and THF, with a rate ($1/\tau_2$) of *ca.* 10^{10} s^{-1}, which did not exist in the nonpolar solvents, *e.g.* 1,4-dioxane and toluene. Accordingly, the new decay pathway indicates the formation of the charge-separated state (CSS), Bodipy$^+$-phenyl-C_{60}^-. With the increase of solvent polarity, the formation rate ($1/\tau_2$) of CSS is visibly increased, *e.g.* 5.62×10^{10} s^{-1} in chlorobenzene, 6.10×10^{10} s^{-1} in dichlorobenzene, and 8.85×10^{10} s^{-1} in THF, all of which are consistent with the previously reported values in similar substances.[33,39] Apparently, the increased rate is correlated with the driving force of the stronger ΔG_{CS} in polar solvents. In spite of this, the formation of CSS plays a subordinate role in completing attenuation processes according to its much lower rate than $1/\tau_1$.

In addition, upon the CSS formation, charge recombination will produce Bodipy-phenyl-$^1C_{60}$*, and then the efficient ISC of the $^3C_{60}$* unit leads to the formation of Bodipy-phenyl-$^3C_{60}$*, as shown in Fig. 4. Besides this CSS attenuation channel, there are several other ISC pathways, such as SOCT-ISC and radical pair ISC (RP-ISC) mechanism.[40,41] In general, the SOCT-ISC mechanism always occurs in an orthogonal geometry with a short linker length between the donor and acceptor. According to the relatively large distance between the electron donor (Bodipy unit) and acceptor (C_{60} unit) in **B-2**, the SOCT-ISC process should be insignificant. However, such a large distance usually means a weak electron exchange between the electron donor and acceptor, thus the RP-ISC might occur along the charge recombination channel of Bodipy$^+$-phenyl-C_{60}^- → Bodipy-phenyl-$^3C_{60}$*. The detailed discussions about the relative

dynamics will be carried out in future and excluded here, according to its subordinate role for attenuation of the excited **B-2**.

3.3 Nanosecond time-resolved transient difference absorption spectra

Once the triplet Bodipy-phenyl-$^3C_{60}$* forms, the bimolecular TTET can occur in the presence of perylene. Fig. 6a shows the nanosecond time-resolved transient absorption spectra of **B-2** in deaerated toluene. The very similar spectra (in Fig. S6–S9, ESI†) were observed in the other deaerated solvents (1,4-dioxane, chlorobenzene, dichlorobenzene and THF). Two positive peaks were observed at 375 and 726 nm, which showed the identical dependence of intensity to delay time. Both of them were attributed to the absorptions of the $^3C_{60}$* unit, according to previous studies.[12,14] An additional experiment was conducted to verify the assignment, where these two band intensities were fast quenched in the presence of solvated oxygen. Therefore, the triplet excited state was exclusively located at the C_{60} unit of **B-2**, as the above inference. Moreover, no GSB of **B-2** at 518 nm was observed, providing another evidence for such efficient and ultrafast energy transfer and ISC processes.

By fitting the attenuation curves of the absorption at 726 nm in the five deaerated solvents (Fig. 6b), the lifetimes of Bodipy-phenyl-$^3C_{60}$* were determined to be 36.7 μs in 1,4-dioxane, 31.8 μs in dichlorobenzene, 30.4 μs in chlorobenzene, 29.5 μs in toluene, and 24.9 μs in THF. A slight decrease of lifetime may originate from self-quenching. As collisions are correlated with solvent viscosities, the diffusion of the photosensitizer became easier with the decrease of viscosity from 1,4-dioxane to THF, resulting in the increase of the self-quenching rate and the reduction of the triplet lifetime.

In the presence of perylene as the triplet acceptor, the transient absorption spectra of **B-2** in deaerated toluene showed visible changes in Fig. 6c. The similar spectra were observed in the other solvents (in Fig. S10–S13, ESI†). Two characteristic absorptions of the $^3C_{60}$* unit at 375 and 726 nm were quickly quenched, while two new bands at 445 and 500 nm clearly appeared. As indicated in the dynamic curves of Fig. 6d, the absorption intensity at 726 nm quickly decreased synchronously with the intensity increasing at 445 and 500 nm within several microseconds after photoexcitation. Then, the two new peaks were both gradually decayed slowly, regardless of the positive

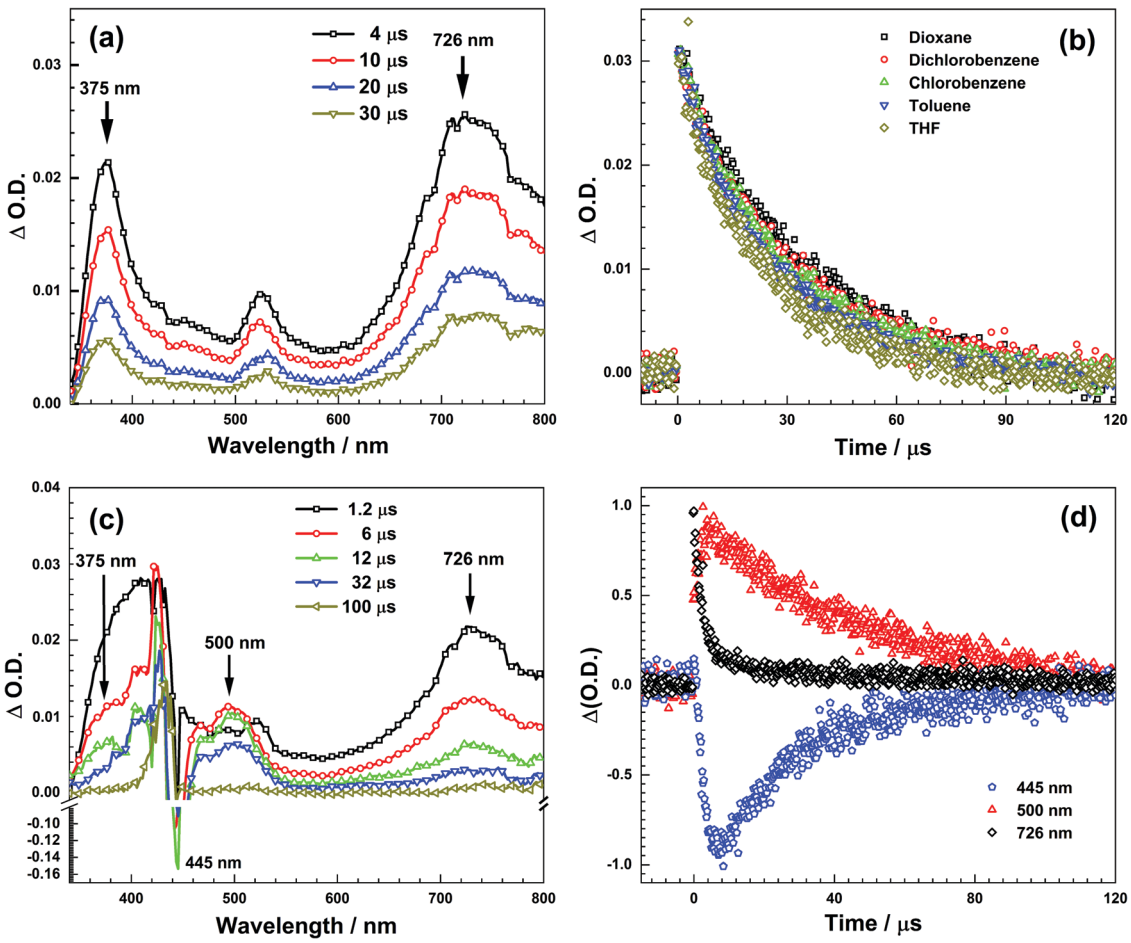

Fig. 6 (a) Nanosecond time-resolved transient absorption spectra of **B-2** in deaerated toluene. (b) Decay curves of the absorption band at 726 nm of **B-2** in five deaerated solvents. (c) Nanosecond time-resolved transient absorption spectra of **B-2** and perylene (c[perylene] = 5×10^{-4} M) in deaerated toluene. (d) Decay curves of the absorption band at 445, 500 and 726 nm of **B-2** and perylene (c[perylene] = 5×10^{-4} M) in deaerated toluene. c[**B-2**] = 1×10^{-5} M, with photoexcitation at 532 nm.

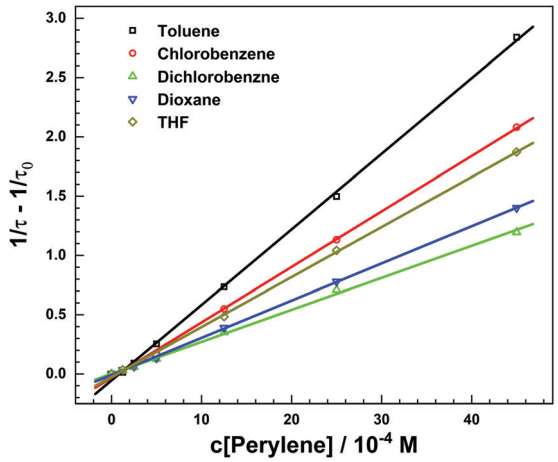

Fig. 7 Stern–Volmer plots for lifetime quenching of the triplet **B-2** with the concentration of perylene in the five deaerated solvents, excited at 532 nm, c[**B-2**] = 1×10^{-5} M.

(500 nm) and negative (445 nm) absorptions. Moreover, the characteristic lifetimes of these two peaks were determined to be 26 μs at 445 nm and 52 μs at 500 nm, respectively, by fitting their decay curves. Consequently, the positive peak at 500 nm was attributed to the absorption of triplet perylene produced by the TTET process. According to the delayed fluorescence emission of perylene itself in the range of 440–525 nm (see Fig. 8), the negative band at 445 nm was assigned to the delayed fluorescence emission of the excited perylene in the S_1 state. The twofold lifetime at 500 nm compared with that at 445 nm exactly matched the TTA mechanism between two triplet perylene molecules.[42]

In addition, using the lifetime of triplet **B-2** derived from fitting the decay curve at 726 nm, the bimolecular quenching rate constant, k_q, was determined by linear-fitting its relationship with perylene concentration using the Stern–Volmer equation (Fig. 7), and all k_q data are summarized in Table 3.

$$1/\tau = 1/\tau_0 + k_q[\text{perylene}] \quad (2)$$

where τ_0 and τ are the lifetimes of triplet **B-2** in the absence and presence of perylene.

In Table 3, the k_q values show a generally opposite trend with solvent viscosity (η), as the TTET process is a typical bimolecular collision reaction. However, these k_q values are much lower than the corresponding diffusion rate constants, k_{dif}. For the **B-2** dyad, the triplet state is located at the C_{60} unit,

Table 3 Bimolecular reaction rate constants (k_q), diffusion rate constants (k_{dif}), and efficiencies of triplet–triplet energy transfer (Φ_{TTET})

Solvent	η (cP)	τ_0 (μs)	k_q (M^{-1} s^{-1})	k_{dif}[a] (M^{-1} s^{-1})	Φ_{TTET}[b]
1,4-Dioxane	1.54	36.7	3.1×10^8	4.2×10^9	0.981
Dichlorobenzene	1.33	31.8	2.7×10^8	4.9×10^9	0.975
Chlorobenzene	0.80	30.4	4.7×10^8	8.1×10^9	0.985
Toluene	0.59	29.5	6.4×10^8	11.0×10^9	0.988
THF	0.55	24.9	4.2×10^8	11.8×10^9	0.979

[a] $k_{dif} = 8k_BT/(3\eta)$. [b] At a perylene concentration of 4.5×10^{-3} M^{-1}.

Table 4 The calculated relative energies of **B-2** and perylene in the lowest singlet and triplet states, in units of eV

Solvent	**B-2** (T_1)	Perylene (S_1)	Perylene (T_1)	ΔE_{TT}[a]	ΔE_{TTA}[b]
1,4-Dioxane	1.569	2.815	1.519	0.050	0.223
Dichlorobenzene	1.540	2.798	1.521	0.019	0.244
Chlorobenzene	1.540	2.802	1.520	0.020	0.238
Toluene	1.569	2.804	1.519	0.050	0.234
THF	1.540	2.819	1.520	0.020	0.221

[a] $\Delta E_{TT} = E_{T_1}$(**B-2**) $- E_{T_1}$(perylene). [b] $\Delta E_{TTA} = 2 \times E_{T_1}$(perylene) $- E_{S_1}$(perylene).

hence the efficient TTET happens only when perylene collides with the dyad from the side of C_{60} unit. Thus, the complex structure of the **B-2** dyad logically reduces the effective collision probability with perylene in solutions, leading to the lower k_q value than k_{dif}. In other words, the overall TTET rate is predominantly limited by the Dexter energy transfer rate in a solvent cage, rather than the diffusion rate. This might be the potential reason for the exception in Table 3 that the k_q value in toluene (6.4×10^8 M^{-1} s^{-1}) is larger than that in THF (4.2×10^8 M^{-1} s^{-1}), although the viscosity of THF is smaller than the toluene one. According to the Dexter mechanism, the TTET rate constant is proportional to the normalized spectral overlap integral at a short collision distance. The spectral overlap integral can be reflected in the triplet energy difference between the donor and acceptor, ΔE_{TT}. Therefore, the ΔE_{TT} changes affected by solvent polarity can significantly influence the TTET rate. As listed in Table 4, the T_1 state of **B-2** is markedly stabilized in chlorobenzene, dichlorobenzene and THF, compared with dioxane and toluene, but no change is visible for the triplet energy of perylene. As a result, ΔE_{TT} becomes considerably larger in dioxane and toluene than in the other solvents. In contrast to the Förster energy transfer, the more positive the ΔE_{TT} value, the greater the driving force for TTET, and thus the more favorable the triplet energy transfer process with the faster quenching rate. Using a relatively high concentration of perylene (4.5×10^{-3} M^{-1}), the TTET quantum yield was calculated by $\Phi_{TTET} = (1/\tau - 1/\tau_0)/(1/\tau)$, and is summarized in Table 3 too.

3.4 TTA upconversion fluorescence spectra

As mentioned above, the delayed fluorescence of the singlet excited perylene was observed in transient absorption spectra of Fig. 6c, implying the effective occurrence of a TTA process. To directly study the TTA kinetics, the fluorescence emission spectra of the mixture solution of **B-2** and perylene with photoexcitation at 532 nm are shown in Fig. 8. The strong blue fluorescence was observed in all five solvents, and the spectra looked very similar to the fluorescence spectra of perylene itself with photoexcitation at 405 nm. For comparison, no fluorescence could be visible in a solution of **B-2** or perylene alone, or an aerated mixed solution of **B-2** and perylene, under photoexcitation at 532 nm. Thus, the emission in Fig. 8 was exclusively attributed to the upconverted fluorescence of singlet excited perylene from the TTA process.

It is well known that the TTA upconversion fluorescence intensity has a quadratic dependence on excitation power at low

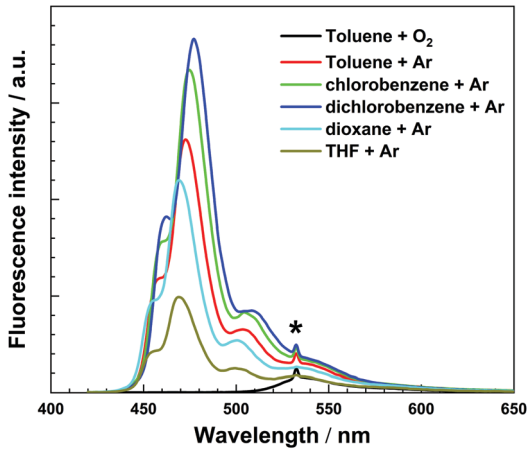

Fig. 8 TTA upconversion fluorescence emission spectra of **B-2** (1×10^{-5} M) and perylene (4.5×10^{-3} M) in different solvents, with photoexcitation at 532 nm (381 mW cm^{-2} power density). Argon was used to deoxygenate in solutions. The asterisks indicate the scattered laser.

intensities and shifts to a linear dependence at higher intensities. The threshold excitation intensity I_{th} of TTA upconversion is an important parameter, at which the incident power dependence is changed from quadratic to linear.[43–45] Therefore, only with the excitation power density higher than I_{th}, the TTA process is the predominant deactivation pathway for the triplet perylene, and the comparison of different solutions becomes valuable.

As shown in Fig. 9a, the upconverted fluorescence intensity increased with the excitation power density. From fitting this dependence in Fig. 9b, the I_{th} values were determined to be 244 mW cm^{-2} in 1,4-dioxane, 226 mW cm^{-2} in dichlorobenzene, 260 mW cm^{-2} in chlorobenzene, 152 mW cm^{-2} in toluene, and 259 mW cm^{-2} in THF. For comparison, the dependence of fluorescence intensity of the light antenna (**B-1**) on excitation power density was also studied (Fig. S20 and S21, ESI†), which showed linear dependence in whole power density range. Thus, all present upconversion experiments were performed with an excitation power density of higher than I_{th} in five solvents, like 381 mW cm^{-2} power density noted in Fig. 8.

It is worth noting that the upconverted fluorescence spectrum presents great dependence on solvents in the range of 440–520 nm. The peak intensity in dichlorobenzene is about four times that in THF. Moreover, the wavelength shifts were also observed in these solvents, which was consistent with the normal fluorescence spectrum of perylene itself (Fig. S19, ESI†). In experiments, the overall TTA upconversion quantum yield (Φ_{UC}) of perylene with **B-2** as the triplet photosensitizer was measured to be 4.9% in 1,4-dioxane, 7.1% in dichlorobenzene, 6.7% in chlorobenzene, 4.6% in toluene, and 2.2% in THF (the maximum of 50%). Apparently, the Φ_{UC} sequence does not completely agree with solvent viscosity or polarity.

Once the triplet perylene is formed, there are two major attenuation pathways. One is the quenching by other molecules, like oxygen, the ground-state perylene, *etc.*, while the other is the TTA process. Thus, the attenuation rate of the triplet perylene concentration can be quantitatively described as eqn (3).

$$\frac{d[^3\text{perylene}^*]}{dt} = -k_T[^3\text{perylene}^*] - k_{TT}[^3\text{perylene}^*]^2 \quad (3)$$

where k_T and k_{TT} are the quenching rate constants of triplet perylene by other molecules and ^{3}perylene* itself, respectively. Usually, the equation can be solved by integration with an initial ^{3}perylene* concentration, then simplified to another expression as eqn (4).[42,44]

$$[^3\text{perylene}^*] = [^3\text{perylene}^*]_0 \frac{1-\beta}{e^{k_T t} - \beta} \quad (4)$$

where the dimensionless parameter β equals the initial fraction of the TTA attenuation rate over the overall decay rate, as eqn (5).

$$\beta = \frac{k_{TT}[^3\text{perylene}^*]_0}{k_T + k_{TT}[^3\text{perylene}^*]_0} \quad (5)$$

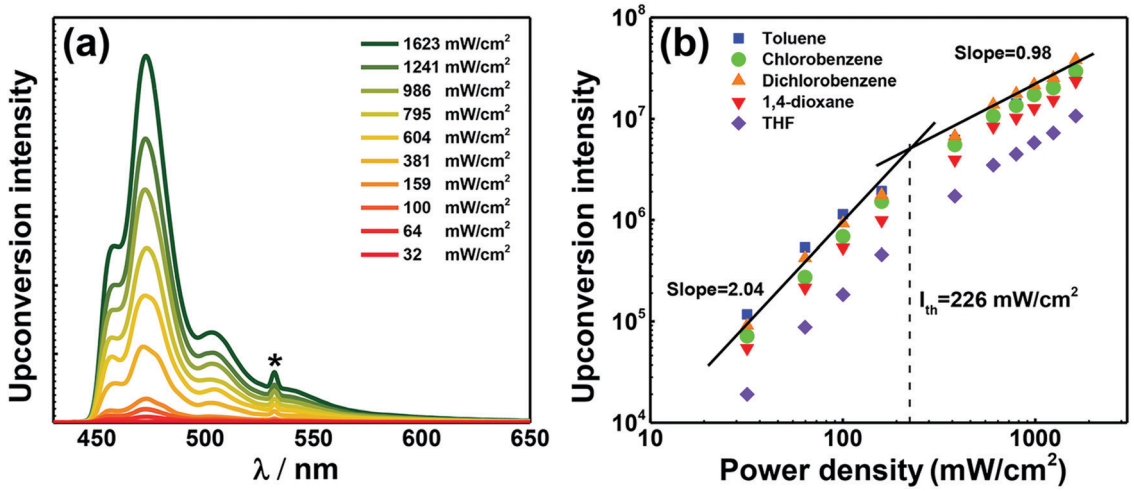

Fig. 9 (a) Dependence of the upconverted fluorescence intensity of perylene (4.5×10^{-3} M) on the excitation power density at 532 nm, with the photosensitizer of **B-2** (1×10^{-5} M) in dichlorobenzene; (b) a double logarithmic plot of integrated TTA upconversion fluorescence intensity of perylene with excitation power density, using **B-2** as the photosensitizer.

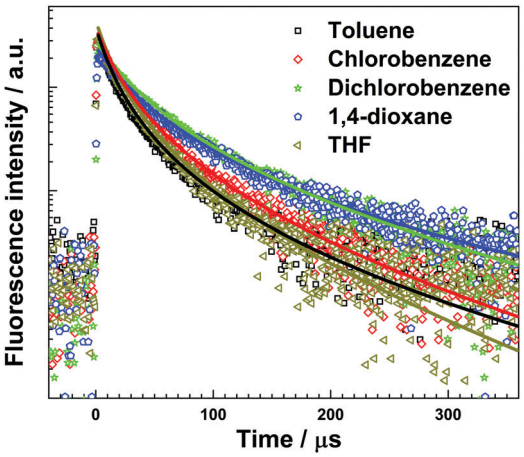

Fig. 10 Time-dependent converted fluorescence intensity of perylene at 470 nm in different solvents, with photoexcitation at 532 nm, 25 °C. c[**B-2**] = 1×10^{-5} M, c[perylene] = 4.5×10^{-3} M.

The time-dependent converted fluorescence intensity, $I_{UC}(t)$, is proportional to the square of triplet perylene concentration, as eqn (6),[46]

$$I_{UC}(t) \propto \left[{}^3\text{perylene}^*\right]^2 = \left[{}^3\text{perylene}^*\right]_0^2 \left(\frac{1-\beta}{e^{k_T t}-\beta}\right)^2 \quad (6)$$

Thus, by fitting the time-dependent converted fluorescence intensity of perylene at 470 nm (Fig. 10), the β values were obtained as 0.925 in 1,4-dioxane, 0.865 in dichlorobenzene, 0.890 in chlorobenzene, 0.931 in toluene, and 0.878 in THF. The proportion of TTA in total attenuation of triplet perylene, f_0, can be calculated to be 0.790 in 1,4-dioxane, 0.687 in dichlorobenzene, 0.727 in chlorobenzene, 0.802 in toluene, and 0.708 in THF, as eqn (7),

$$f_0 = -\left[{}^3\text{perylene}^*\right]_0^{-1} \int_0^\infty k_{TT} \left[{}^3\text{perylene}^*\right]_t^2 dt = 1 - \frac{\beta - 1}{\beta} \ln(1-\beta) \quad (7)$$

According to the spin-statistical law,[47,48] interaction of two acceptor triplets can produce up to nine excited state dimer spin states with equal probability. These nine encounter-pair spin states can classify into three distinct sublevels, five quintet (S = 2), three triplet (S = 1), and one singlet (S = 0) character. Thus, we could expect that the upconverted fluorescence from TTA represents 0.11 of the annihilation events. However, this statistical factor f can be further enlarged to 0.4, when taking into account the dissociation of a quintet encounter-pair to two triplets. Thus, the TTA quantum yields, Φ_{TTA}, defined as $\Phi_{TTA} = f \times f_0$, were calculated and are listed in Table 5.

As indicated in Table 5, no obvious correlation between solvent viscosity and TTA quantum yield was found, although the solvent viscosity should be crucial for such bimolecular reactions. As we mentioned previously,[24] the energy gap ΔE_{TTA} between the singlet energy and twofold the energy of triplet also played an important role in TTA rate. The smaller the positive ΔE_{TTA} value, the more favorable the TTA process.[15] Thus, the ΔE_{TTA} values in the five solvents were calculated and are listed in Table 4 too. In general, the consistent trend can be found when considering solvent viscosity and ΔE_{TTA} values together. For instance, dichlorobenzene and 1,4-dioxane have the similar viscosity, but the greater ΔE_{TTA} in dichlorobenzene causes the higher TTA quantum yield than in 1,4-dioxane. We would like to emphasize that all data of Φ_{TTA}, as well as Φ_{ET}, Φ_{ISC}, and Φ_{TTET}, are relatively close in the five solvents. Therefore, the fluorescence quantum yield Φ_{FL} of perylene itself in five solvents is expected to be the most crucial factor for the overall TTA upconversion process.

Table 5 The quantum yields of intramolecular energy transfer (Φ_{ET}), intersystem crossing (Φ_{ISC}), triplet–triplet energy transfer (Φ_{TTET}), triplet–triplet annihilation (Φ_{TTA}), and fluorescence emission (Φ_{FL}) of perylene with the **B-2** photosensitizer, as well as the calculated and experimental upconversion quantum yields (Φ_{UC})

				Φ_{TTA}[a]			Φ_{UC}[d] (%)	
Solvent	Φ_{ET}	Φ_{ISC}	Φ_{TTET}	$f_1 \times f_0$	$f_2 \times f_0$	Φ_{FL}[b]	Cal.[c]	Exp.
1,4-Dioxane	0.995	0.95	0.981	0.088	0.316	0.569	2.3 (8.3)	4.9
Dichlorobenzene	0.993	0.95	0.975	0.076	0.275	0.786	2.8 (9.9)	7.1
Chlorobenzene	0.993	0.95	0.985	0.081	0.291	0.657	2.4 (8.9)	6.7
Toluene	0.996	0.95	0.988	0.089	0.321	0.501	2.1 (7.5)	4.6
THF	0.996	0.95	0.979	0.079	0.283	0.442	1.6 (5.8)	2.2

[a] Φ_{TTA} can be calculated as $f \times f_0$ in theory, where f_1 is 0.11 and f_2 is 0.4. [b] Fluorescence quantum yields of perylene (1×10^{-4} M) were measured with photoexcitation at 405 nm, using that of perylene in cyclohexane as the standard (Φ_{FL} = 0.73).[49] [c] $\Phi_{UC} = 1/2 \cdot \Phi_{ET} \cdot \Phi_{ISC} \cdot \Phi_{TTET} \cdot \Phi_{TTA} \cdot \Phi_{FL}$ using f_1 = 0.11, while the values in parentheses were calculated with f_2 = 0.4. [d] The maximal upconversion quantum yield is set as 50%.

3.5 Fluorescence quantum yield of perylene

Although perylene is a very popular triplet acceptor in a TTA upconversion system due to its S_1 state energy close to twofold T_1 energy, its optimized concentration for TTA upconversion has been rarely mentioned. A higher concentration is favorable for saturating the TTET process, but too high concentration will cause more significant self-absorption or formation of an excimer or exciplex. Therefore, a relatively low concentration of 1×10^{-4} M was cautiously chosen in present investigation, but it was necessary to keep a near unity Φ_{TTET} in Table 5. Moreover, using photoexcitation at 405 nm, the fluorescence quantum yield of perylene, Φ_{FL}, was measured in the five solvents to check its dependence on solvent polarity. As listed in Table 5, the Φ_{FL} value of perylene was determined to be 0.569 in 1,4-dioxane, 0.786 in dichlorobenzene, 0.657 in chlorobenzene, 0.501 in toluene, and 0.442 in THF. Apparently, dichlorobenzene shows the best performance for the fluorescence emission of perylene in the S_1 state. This conclusion generally agrees with our previous study[24] that the yield showed a consistent trend with solvent polarity, among hexane, heptane, toluene, and 1,4-dioxane. However, these phenomena are not strong evidence enough to build a certain relationship among the Φ_{FL} and solvent properties.

We have tried to assess the general solvent effects using the Lippert–Mataga theory,[50,51] taking into account second order effects, such as the dipole moments induced in the solvent molecules resulting from the excited fluorophore, and *vice versa*. To our satisfaction, the calculated interactions were

basically consistent with Φ_{FL} except for THF. Moreover, in addition to solvent polarity, several solvent effects like hydrogen bonding and the formation of an excimer or exciplex can also affect the Φ_{FL} value of perylene significantly. In the view of the molecular structures of these solvents, hydrogen bonds could be readily formed between perylene and chloride solvents, like chlorobenzene and dichlorobenzene, which would efficiently enhance the fluorescence of perylene in the S_1 state. Among the present five solvents, THF is an exception, since it has the strongest interaction according to the Lippert–Mataga theory, but its Φ_{FL} is the lowest in Table 5. In the recent Ye *et al.*'s experiment,[22] a similar phenomenon was also observed. More detailed theoretical and experimental investigations are needed to illuminate the exception.

3.6 Overall TTA upconversion quantum yield

As shown in Fig. 1a, the overall TTA upconversion quantum yield Φ_{UC} can be calculated as eqn (8). Table 5 summarizes the calculated results based on the obtained quantum yield for each elementary reaction.

$$\Phi_{UC} = \Phi_{ET}\cdot\Phi_{ISC}\cdot\Phi_{TTET}\cdot\Phi_{TTA}\cdot\Phi_{FL} \quad (8)$$

Using the statistical spin factor f_1 of 0.11, the calculated Φ_{UC} values are less than a half of the experimental data in the five solvents, while those with f_2 = 0.4 are generally higher. This indicates that the dissociation of a quintet encounter-pair to two triplets is indispensable when the encounters of the triplet pair are formed in the title system. Moreover, the significant solvent effects observed in current experiments were mainly determined by the fluorescence quantum yield, which provided the most crucial factor for us to choose solvent in future works with perylene as the triplet acceptor.

4 Conclusions

In this work, we have studied the TTA upconversion kinetics of perylene with **B-2** as the triplet photosensitizer in five solvents, 1,4-dioxane, dichlorobenzene, chlorobenzene, toluene, and THF. The influences of solvent viscosity and polarity were cautiously checked in each elementary reaction involved in the TTA upconversion kinetics.

Although no significant solvent effect was observed in steady-state absorption and fluorescence emission spectra, the overall TTA upconversion quantum yields showed a profound dependence on solvent properties. With the aid of the femtosecond time-resolved transient absorption spectra of the light antenna of **B-2** after photoexcitation at 532 nm, the lowest triplet state was confirmed to be formed by intramolecular Förster energy transfer and ISC, and located on the C_{60} unit. Moreover, an extra intramolecular energy-transfer pathway of **B-2** was verified by CV analysis, in which a charge-separated state intermediate could be formed in dichlorobenzene, chlorobenzene, and THF solvents, once being excited. However, the new energy transfer pathway was subordinate due to a much slower rate.

In bimolecular reactions like TTET and TTA processes, the solvent viscosity usually plays an important role. The prolonged lifetime of the triplet **B-2** itself was consistent with the increase of solvent viscosity indeed. However, in the presence of perylene, the TTET rate constant between the triplet **B-2** and perylene in five solvents did not agree with the trend of viscosity. The unpredictable result strongly indicates that the more positive ΔE_{TT} value is favorable for the triplet energy transfer from the triplet photosensitizer to the acceptor. Moreover, both the viscosity and the ΔE_{TTA} value showed considerable effects on the TTA yield of perylene when using **B-2** as the photosensitizer in the five solvents. To our surprise, the fluorescence emission of perylene was significantly affected by solvents in contrast to the other steps, which caused the obvious solvent effects on the overall TTA upconversion of the title system. In addition, the calculated and experimental TTA upconversion quantum yields in the five solvents implied that the dissociation of a quintet encounter-pair to two triplets is considerable in this system. These conclusions provide useful clues to choose the most favorable solvent for the higher TTA upconversion efficiency in the related applications.

Conflicts of interest

There are no conflicts to declare.

Acknowledgements

This work was supported by the National Natural Science Foundation of China (Grant No. 21873089, 11974381, and 11674355) and the National Key Research and Development Program of China (No. 2019YFA0307700). The quantum chemical calculations in this study were performed on the supercomputing system in Supercomputing Center of USTC.

References

1 M. P. Rauch and R. R. Knowles, *Chimia*, 2018, **72**, 501–507.
2 V. Gray, D. Dzebo, M. Abrahamsson, B. Albinsson and K. Moth-Poulsen, *Phys. Chem. Chem. Phys.*, 2014, **16**, 10345–10352.
3 M. Majek, U. Faltermeier, B. Dick, R. Perez-Ruiz and A. Jacobi von Wangelin, *Chem. – Eur. J.*, 2015, **21**, 15496–15501.
4 Y. Wei, Y. Li, M. Zheng, X. Zhou, Y. Zou and C. Yang, *Adv. Opt. Mater.*, 2020, **8**, 1902157.
5 X. Yang, X. Wu, D. Zhou, J. Yu, G. Xie, D. W. Bruce and Y. Wang, *Dalton Trans.*, 2018, **47**, 13368–13377.
6 J. Zhao, S. Ji, W. Wu, W. Wu, H. Guo, J. Sun, H. Sun, Y. Liu, Q. Li and L. Huang, *RSC Adv.*, 2012, **2**, 1712–1728.
7 J. Yu, M. Li, C. Xu, F. Meng, J. Cao, H. Tan and W. Zhu, *Dalton Trans.*, 2020, **49**, 8785–8790.
8 J. Yu, M. Xiao, H. Tan and W. Zhu, *Thin Solid Films*, 2016, **619**, 1–9.
9 J. Zhao, S. Ji and H. Guo, *RSC Adv.*, 2011, **1**, 937–950.
10 J. Zhao, W. Wu, J. Sun and S. Guo, *Chem. Soc. Rev.*, 2013, **42**, 5323–5351.
11 M. K. Manna, S. Shokri, G. P. Wiederrecht, D. J. Gosztola and A. J. Ayitou, *Chem. Commun.*, 2018, **54**, 5809–5818.

12 Y. Wei, M. Zhou, Q. Zhou, X. Zhou, S. Liu, S. Zhang and B. Zhang, *Phys. Chem. Chem. Phys.*, 2017, **19**, 22049–22060.
13 Y. Wei, M. Zheng, Q. Zhou, X. Zhou and S. Liu, *Org. Biomol. Chem.*, 2018, **16**, 5598–5608.
14 P. Yang, W. Wu, J. Zhao, D. Huang and X. Yi, *J. Mater. Chem.*, 2012, **22**, 20273.
15 V. Gray, D. Dzebo, A. Lundin, J. Alborzpour, M. Abrahamsson, B. Albinsson and K. Moth-Poulsen, *J. Mater. Chem. C*, 2015, **3**, 11111–11121.
16 F. Zhong and J. Zhao, *Dyes Pigm.*, 2017, **136**, 909–918.
17 Y. Murakami, T. Ito and A. Kawai, *J. Phys. Chem. B*, 2014, **118**, 14442–14451.
18 Y. Murakami, H. Kikuchi and A. Kawai, *J. Phys. Chem. B*, 2013, **117**, 2487–2494.
19 K. Yokoyama, Y. Wakikawa, T. Miura, J. Fujimori, F. Ito and T. Ikoma, *J. Phys. Chem. B*, 2015, **119**, 15901–15908.
20 C. Mongin, J. H. Golden and F. N. Castellano, *ACS Appl. Mater. Interfaces*, 2016, **8**, 24038–24048.
21 V. Gray, A. Dreos, P. Erhart, B. Albinsson, K. Moth-Poulsen and M. Abrahamsson, *Phys. Chem. Chem. Phys.*, 2017, **19**, 10931–10939.
22 C. Ye, V. Gray, J. Martensson and K. Borjesson, *J. Am. Chem. Soc.*, 2019, **141**, 9578–9584.
23 S. Vyas and P. K. Sharma, *J. Chem. Sci.*, 2002, **114**, 137–148.
24 Q. Zhou, M. Zhou, Y. Wei, X. Zhou, S. Liu, S. Zhang and B. Zhang, *Phys. Chem. Chem. Phys.*, 2017, **19**, 1516–1525.
25 Y. Zhou, F. N. Castellano, T. W. Schmidt and K. Hanson, *ACS Energy Lett.*, 2020, **5**, 2322–2326.
26 M. Frisch, G. Trucks, H. B. Schlegel, G. Scuseria, M. Robb, J. Cheeseman, G. Scalmani, V. Barone, B. Mennucci and G. Petersson, *Gaussian 09*, Gaussian. Inc., Wallingford, CT, 2009.
27 C. Reichardt and T. Welton, *Solvents and solvent effects in organic chemistry*, John Wiley & Sons, 2011.
28 S. Nath, H. Pal, D. K. Palit, A. V. Sapre and J. P. Mittal, *J. Phys. Chem. B*, 1998, **102**, 10158–10164.
29 M. Terazima, N. Hirota, H. Shinohara and Y. Saito, *J. Phys. Chem.*, 1991, **95**, 9080–9085.
30 V. Biju, T. Itoh, Y. Baba and M. Ishikawa, *J. Phys. Chem. B*, 2006, **110**, 26068–26074.
31 S. Shao, M. B. Thomas, K. H. Park, Z. Mahaffey, D. Kim and F. D'Souza, *Chem. Commun.*, 2018, **54**, 54–57.
32 R. Ziessel, B. D. Allen, D. B. Rewinska and A. Harriman, *Chemistry*, 2009, **15**, 7382–7393.
33 V. Bandi, H. B. Gobeze, V. Lakshmi, M. Ravikanth and F. D'Souza, *J. Phys. Chem. C*, 2015, **119**, 8095–8102.
34 C. O. Obondi, G. N. Lim, P. A. Karr, V. N. Nesterov and F. D'Souza, *Phys. Chem. Chem. Phys.*, 2016, **18**, 18187–18200.
35 R. Ziessel, B. D. Allen, D. B. Rewinska and A. Harriman, *Chem. – Eur. J.*, 2009, **15**, 7382–7393.
36 J. W. Arbogast, A. P. Darmanyan, C. S. Foote, F. N. Diederich, R. Whetten, Y. Rubin, M. M. Alvarez and S. J. Anz, *J. Phys. Chem.*, 1991, **95**, 11–12.
37 J. Hou, A. Zhao, T. Huang and S. Lu, *Encyclopedia of Nanoscience and Nanotechnology*, American Scientific Publishers, 2004, vol. 1, pp. 409–474.
38 J. W. Arbogast and C. S. Foote, *J. Am. Chem. Soc.*, 1991, **113**, 8886–8889.
39 M. E. El-Khouly, A. N. Amin, M. E. Zandler, S. Fukuzumi and F. D'Souza, *Chem. – Eur. J.*, 2012, **18**, 5239–5247.
40 Y. Hou, X. Zhang, K. Chen, D. Liu, Z. Wang, Q. Liu, J. Zhao and A. Barbon, *J. Mater. Chem. C*, 2019, **7**, 12048–12074.
41 Z. Wang and J. Zhao, *Org. Lett.*, 2017, **19**, 4492–4495.
42 T. W. Schmidt and F. N. Castellano, *J. Phys. Chem. Lett.*, 2014, **5**, 4062–4072.
43 A. Monguzzi, J. Mezyk, F. Scotognella, R. Tubino and F. Meinardi, *Phys. Rev. B: Condens. Matter Mater. Phys.*, 2008, **78**, 195112.
44 A. Haefele, J. Blumhoff, R. S. Khnayzer and F. N. Castellano, *J. Phys. Chem. Lett.*, 2012, **3**, 299–303.
45 Y. Wei, M. Zheng, L. Chen, X. Zhou and S. Liu, *Dalton Trans.*, 2019, **48**, 11763–11771.
46 Y. Y. Cheng, B. Fückel, T. Khoury, R. G. Clady, M. J. Tayebjee, N. Ekins-Daukes, M. J. Crossley and T. W. Schmidt, *J. Phys. Chem. Lett.*, 2010, **1**, 1795–1799.
47 A. Monguzzi, R. Tubino, S. Hoseinkhani, M. Campione and F. Meinardi, *Phys. Chem. Chem. Phys.*, 2012, **14**, 4322–4332.
48 T. Ogawa, N. Yanai, A. Monguzzi and N. Kimizuka, *Sci. Rep.*, 2015, **5**, 10882.
49 J. Olmsted, *J. Phys. Chem.*, 1979, **83**, 2581–2584.
50 E. Z. V. Lippert, *Zeitschrift für Elektrochemie, Berichte der Bunsengesellschaft für physikalische Chemie*, 1957, **61**, 962–975.
51 N. Mataga, Y. Kaifu and M. Koizumi, *Bull. Chem. Soc. Jpn.*, 1956, **29**, 465–470.

